RESEARCH ARTICLE

THE EFFECT of MINOR Ti and Sr ADDITION on the MICROSTRUCTURAL, MECHANICAL, and CORROSION PROPERTIES of a BIODEGRADABLE Mg-5Sn-3Al ALLOY

Selma ÖZARSLAN*

*Hatay Mustafa Kemal University, Faculty of Arts and Sciences, Department of Physics, selmaozarsln@gmail.com,
ORCID: 0000-0002-7225-1613

ABSTRACT

In this study, the microstructural, mechanical, and corrosion properties of the alloys obtained by adding Al-15Ti and Al-15Sr master alloys to the Mg-5Sn alloy were investigated. Microstructural properties of the alloys were investigated by X-ray diffraction (XRD), scanning electron microscopy (SEM), and optical microscopy (OM). The mechanical properties of the alloys were analyzed by performing tensile tests, macrohardness tests, and nanoindentation tests. Corrosion behavior of both alloys was investigated by determining the corrosion rates with both electrochemical techniques and immersion techniques in Hanks Balanced Salt Solution (HBSS). When the microstructure results were examined, it was observed that minor Ti and Sr have a significant effect on reducing magnesium grain size, with Ti being more effective in grain refining. When compared to Al-15Sr, the addition of Al-15Ti to Mg-5Sn improves both mechanical and corrosion properties more effectively.

1. INTRODUCTION

The use of magnesium as a biomaterial dates back many years ago, and it has again found a field of application along with the development of technology. In the field of health, magnesium, which was discovered by Humphrey Davy in 1808, is used in implant applications due to its biodegradable property. Mg wires were initially used by Dr. Edward C. Huse in 1878 to join the veins in order to stop the bleeding of patients [1-3]. Later, it was decided to abstain from using pure magnesium as a biomaterial due to its weak mechanical property and high corrosion rate, and stainless steel has begun to be used [2,4]. But by the studies conducted, it was observed that the weak mechanical properties and high corrosion rate of magnesium were improved by the addition of alloy elements, and for about 20 years, it has found an extensive field of application in the health sector as a biodegradable metallic alloy [5].

Magnesium alloys exhibit superior properties in many aspects compared to other biodegradable metallic alloys (like iron and zinc-based alloys).   Even though Fe, and Fe-based alloys have high strength and high biocompatibility, their elastic modulus is much higher than the elastic modulus of human bone, and this status causes the fact of stress concentration frequently encountered in metallic

implants. Thus, the area of use of Fe and Fe-based alloys is limited [6]. Similarly, the corrosion rate of zinc, which is a biodegradable metallic material, has a value between the Fe and Mg-based alloys. But as the intake of zinc of more than 100-300 mg per day causes severe health problems, it requires the selection of alloy to be made carefully [7]. The corrosion resistance of pure magnesium is able to be improved by the addition of various alloy elements [4]. However, care must be taken to ensure that the alloy elements are especially biocompatible and do not have toxic effects [7-8]. As tin (Sn) is among the main elements present in the human body, its use in the field of biomaterials has become widespread [9]. Thus, Mg-Sn has been determined as the main alloy in this study. When the studies conducted on Mg-Sn alloy, as a biodegradable alloy, were examined, Gu et al. [7] examined the corrosion and biocompatibility of Mg-1Sn alloy and asserted that Sn may be a good alloy element for magnesium alloys. And in a study conducted on the addition of different weight rates of Sn to magnesium, it was found that the Mg-5Sn alloy has the best mechanical properties [10]. For this reason, Sn was used at a rate of 5% by weight in this study.

When the studies conducted were examined, it was observed that the studies for improving the properties of biodegradable Mg-based alloys had concentrated on the AZ series (with aluminum and zinc as alloy elements). As the addition of Al to magnesium increases the tensile strength and forms an Al_2O_3 oxide layer on the surface of the alloy as it reduces the grain size of the alloy, it was observed that it also increases the corrosion resistance [11-12]. Moreover, it was reported that a small amount of aluminum continuously released along with the degradation process in the body could be tolerated [13-15]. Huang et al. [16], in their study conducted on Mg-Sn-Al alloys, found that Mg-3.52Sn-3.32Al alloy exhibits better mechanical properties compared to AZ31B, and that Mg-6.54Sn-4.78Al alloy exhibits better mechanical properties compared to ZK60. Moreover, in their study, Bowles et al. [17] presented a preliminary examination with respect to the Mg-Sn(-Al) alloy system. As the Mg-Sn-based alloys have good creep properties and high corrosion resistance, and as tin is a very cheap alloy element and has a low melting point and increases castability, it was observed that the studies concentrated on this main alloy.

In this study, Al-5Ti and Al-15Sr master alloys, functioning as grain refiners, were used for the addition of Al to Mg-5Sn alloys. Thus, the effect of the addition of minor Ti and Sr to Mg-5Sn-3Al alloys on microstructural, mechanical, and corrosion properties was investigated. Koltygin et al. [18] added Al–5Ti–1B to the AZ91 alloy and examined its effect on the mechanical properties of the alloy. The results showed that the Al–5Ti–1B master alloy improves the mechanical properties of the AZ91 magnesium alloy. The production of Mg-5Sn-3Al-0,3Ti (TA-Ti) and Mg-5Sn-3Al-0,4Sr (TA-Sr) alloys obtained by the addition of Al-6Ti and Al-15Sr master alloys to Mg-5Sn alloy was performed by the use of die casting machine. By this production technique, the performance of fine grain size, high-strength and very thin-walled castings becomes possible [19-20]. Thus, the improvement of both the mechanical properties and corrosion resistance of fine-grained alloys is enabled [21-23]. In this study, it was intended to examine the microstructural, mechanical, and corrosion properties of new alloys produced using two different master alloys, and to determine the alloy having better mechanical and corrosion properties.

2. MATERIAL AND METHOD

2.1. Production of the Materials

To produce Mg-5Sn-3Al-0,3Ti (TA-Ti) and Mg-5Sn-3Al-0,4Sr (TA-Sr) alloys, high purity Al-5Ti and Al-15Sr master alloys were added to molten Mg-5Sn by calculating mass weight ratios. Both

alloys were produced using the high pressure die casting (HPDC) technique. The production of alloys used in this study was performed using 96% CO_2 and 4% SF_6 gas mixture in a silicon carbide melting pot in an induction melting furnace having a power of 1.5 kW. In the production of the alloys, Mg with a purity of 99.8%, Sn with a purity of 99.8%, and as a grain refiner, the Al-15Ti and Al-15Sr master alloys of 3% by weight were used. For each alloy, the solution was held at a temperature of 750 $^{\circ}$C for 10 minutes. After holding, mixing was performed in a shielding gas environment, and the production was performed in a cold chamber die casting machine with a 100-ton capacity and cold chamber high-pressure die-cast machine with 76kN injection force.

For the whole analyses, the samples produced were removed from the casting centers with wire erosion in the form of cylinder with a diameter of 10 mm and a thickness of 2 mm. Before all the microstructure analyses, the surfaces of the alloys were first subjected to grinding operations with 800, 1200, 2500, and 4000 grit papers, and then to polishing operations with 1μm alumina wax. Right after the polishing operation, the surfaces of the samples were washed with pure water and alcohol, then dried. For the grain structures of the alloys and arising intermetallic phases to become apparent, the surfaces of the samples were seared with Nital (2% nitric acid and 98% ethyl alcohol).

2.2. Microstructure Characterization

Microstructure analyses of alloys produced by the HPDC method were performed by the use of optical microscopy (OM), scanning electron microscopy (SEM) analysis, and X-ray diffraction (XRD) analysis. XRD analyses were performed by the use of a Rigaku brand Smartlab model X-ray diffractometer under Cu-Kα radiation, 40 kV voltage, and 30 mA current with a 1 degree/min. measurement rate in the range of 0 and 90 degrees, and phase identification was carried out according to the ICDD database. An Olympus brand BX51 model OM device was used for the microstructure images of the samples, whose metallographic sample preparation operations were completed. AnalySIS Pro Software (Olympus Soft Imaging Solutions, Germany) was used for grain size measurements.

2.3. Mechanical Characterization

In the hardness calculation of the samples, nanoindentation and macrohardness tests were performed. As a result of the nanoindentation tests of the alloys, reduced elastic modulus (E_r) and nanohardness (H_N) values were determined. Hysitron TI 950 TriboIndenter device was used for the tests. Following the nanoindentation measurement, the images of the surface were recorded as before and after the hardness test by the scanning probe microscopy (SPM) for the surface analysis. Diamond Berkovich was used as hardness tip. The tests were performed in load-controlled feedback mode, and through the application of 6 units of load on a matrix of 3x2 formed on the surface under a force of maximum 5 mN, and in 5 seconds of loading and unloading periods, and 2 seconds of waiting periods. The applied load and displacement data obtained after the measurement was analyzed according to the Oliver-Pharr method. By this method, the samples' nanohardness and elastic modulus values are able to be determined from the loading and unloading curve [24]. And the macrohardness measurements of the materials were performed with the Brinell hardness device. In order to determine the hardness, the sample's Brinell hardness value was calculated by measuring the diameter of the mark formed on the sample's surface by the tip.

The alloys' tensile tests were performed with RAAGEN brand universal tensile machine. The tensile tests of each alloy were performed by averaging over 4 samples. The tensile tests, using rectangular

test specimens in accordance with ASTM standard E8/E8M were performed at a body temperature of 36.5 $^{\circ}$C and at a pulling speed of 0.2 mm/min.

2.4. Corrosion Tests

Both electrochemical and immersion tests were performed to examine the corrosion behavior of the alloys. Electrochemical corrosion tests were performed with a potentiostat/galvanostat device (CH Instruments). The tests were performed with the use of the samples in which three electrode systems were used, namely the Ag/AgCl reference electrode, the platinum counter electrode, and the working electrode. All the corrosion tests were performed in 100 ml of HBSS prepared by simulating the body fluid. Some corrosion parameters were obtained by fitting the Tafel curves obtained from electrochemical tests, and corrosion rates were calculated. As a result of the immersion tests of the alloys, the measured mass loss weights and degradation rates were calculated. The immersion tests were performed again in 100 ml of HBSS with measurements at specific time intervals.

3. RESULTS

Figure 1 shows the (a) OM and (b) SEM microstructures and grain sizes of TA-Ti and TA-Sr alloys. As observed in Figure 1, the grain size of the titanium added alloy was measured as 13.7 μm, and the grain size of the strontium added alloy was measured as 23.6 μm. Through both the grain size measurements and SEM and OM images, it may be said that the titanium element is more effective in grain refining. When the XRD graph of TA-Ti and TA-Sr alloys given in Figure 2 is examined, Mg_2Sn eutectic phase has formed on the grain boundaries observed in SEM images of the alloys as well as the primary α-Mg. The microstructure of both alloys indicated that the grains and secondary phases (Mg_2Sn) had showed a homogenous distribution. As shown in Figure 1 (b), residues were observed at grain borders verified by X-ray diffraction analysis. As Al decomposes in α-Mg matrix due to trace addition of Ti and Sr, and due to the addition of Al of less than 3% by weight, the formation of a new phase is not expected. Considering the Mg-Al binary equilibrium diagram, the decomposition rate of Al in Mg is 25 at room temperature [25]. As the production method ensures rapid solidification, the formation of a beta phase is not expected. This status was also revealed by the XRD analysis.
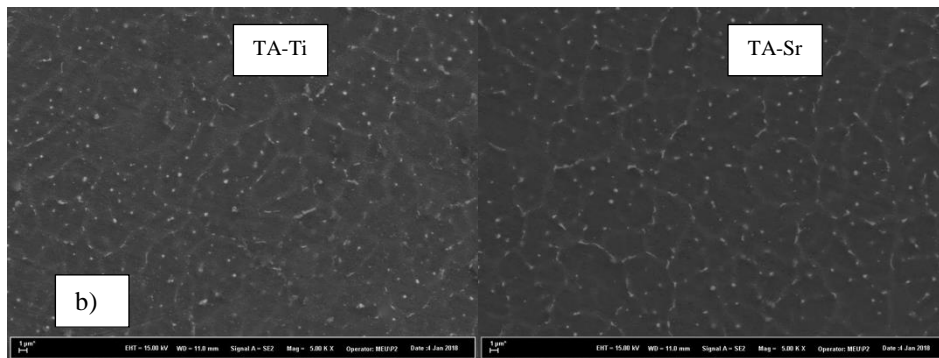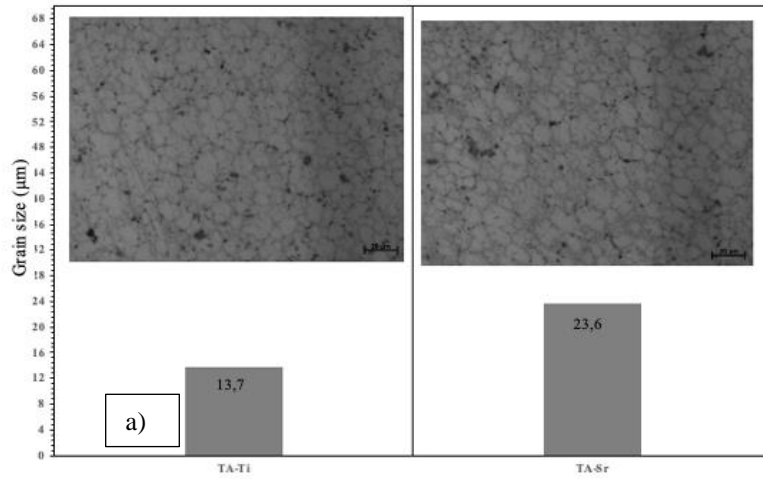
Figure 1. (a) Grain size distribution graph and OM images; **(b)** SEM images of TA-Ti and TA-Sr magnesium alloys.
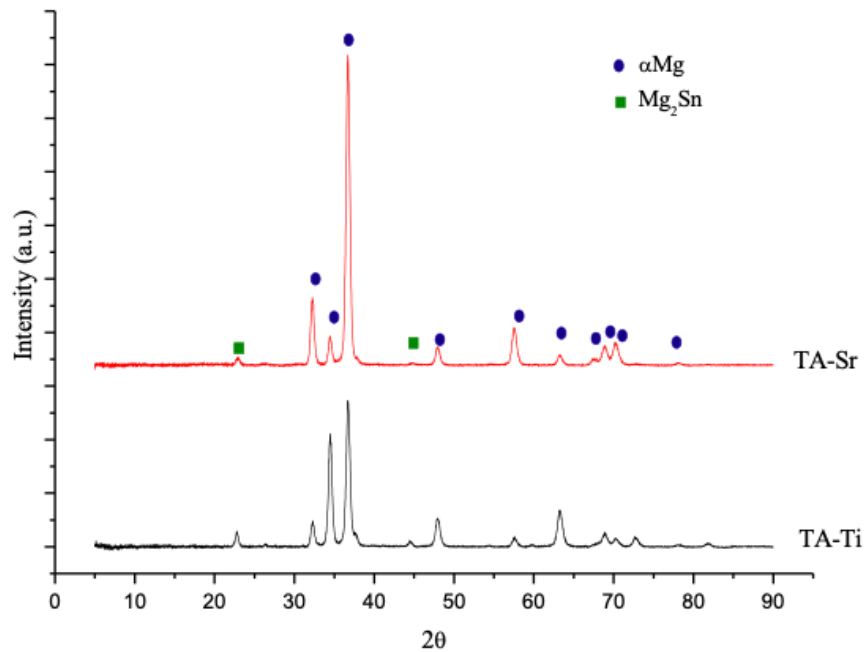
Figure 2. XRD analysis of TA-Ti and TA-Sr magnesium alloys.

In Figure 3, percentage elongation, tensile strength, yield strength, and hardness values of TA-Ti and TA-Sr alloys are observed. The percentage elongation, yield strength, tensile strength, and macrohardness values of TA-Ti alloys are 15.2, 150 MPa, 203 MPa, and 50 HB, respectively, and they are 10.4, 135 MPa, 197 MPa, and 50 HB, respectively, for the TA-Sr alloy. The demonstration of better mechanical properties by the TA-Ti alloy may be associated with the more effective grain size reduction by the addition of titanium. Because the reduction of grain size is one of the mechanisms that increases strength [26]. With the reduction of grain size, the amount of grain boundary increases. In this case, it causes the formation of an impediment, which limits the movements of the dislocations. When the grain size graph in Figure 1(a) and the macrohardness values in Figure 3 are compared, it is observed that the alloy in which Ti was added exhibits higher mechanical properties. Ti is known as a strong structural cooling element. Ti atoms limit the growth of α-Mg and cause the formation of a finer-grained microstructure, and in addition, when Ti is used as the active component of the refiner, it accelerates the nucleation [27, 28]. Moreover, the homogenous precipitation of secondary particles contributes to high macrohardness [29].
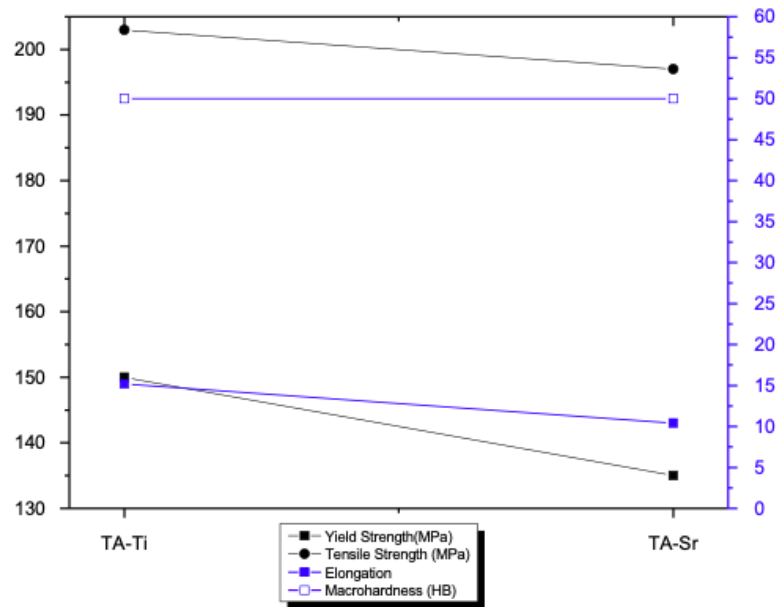
Figure 3. Percentage elongation, tensile strength, yield strength, and macrohardness graph of TA-Ti and TA-Sr alloys.

In Figure 4, the load-displacement curves applied on TA-Ti and TA-Sr alloys are given. As observed from the OM images of the alloys, the fact of *pop-in* is not observed in the curves due to the homogenous structure of the alloys. By the calculations obtained from the load-displacement curves, the average nanohardness and elastic modulus values for the TA-Ti alloy were found to be 46 GPa and 1.19 GPa, respectively, and they were found to be 45.6 GPa and 1.12 GPa for the TA-Sr alloy. Considering these values, it was observed that the nanohardness and elastic modulus were barely increased by the addition of Ti. The increase in the nanohardness value may be directly attributed to the change in microstructure. The increase in nanohardness value by the addition of Ti might have arisen due to the limiting effect of the reduction in grain size on the dislocation movement. On the other hand, it may not be possible to associate the cause of the change in elastic modulus directly with the change in microstructure [30, 31]. The studies performed didn't show that the alloy elements being present in small or trace amounts in the matrix of such alloys affect the magnesium towards higher elastic modulus values [32].
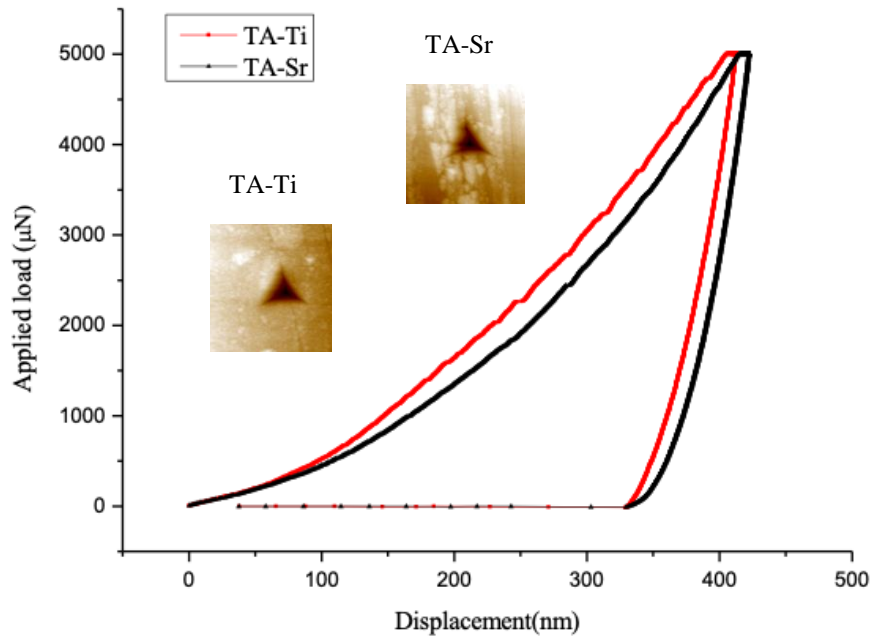
Figure 4. Load-displacement curves of TA-Ti and TA-Sr magnesium alloys.

In Figure 5, the Tafel curves of TA-Ti and TA-Sr alloys obtained from the potentiodynamic polarization test performed in HBSS are given. The addition of Al-15Sr as 3% by weight to the Mg-5Sn alloy caused the alloy's corrosion potential value to move more in a positive direction compared to addition of Al-15Ti as 3% by weight. In Table 1, the corrosion parameters obtained from the Tafel curves of the alloys are given. When Table 1 is examined, the current density values of TA-Ti and TA-Sr alloys were measured as 4.45 $\mu A.cm^{-2}$ and 6.80 $\mu A.cm^{-2}$, respectively, and their corrosion rates were measured as 3.8 mm/yr and 5.8 mm/yr. In this case, it was observed that the addition of Ti is more effective in increasing the corrosion resistance of the TA main alloy.
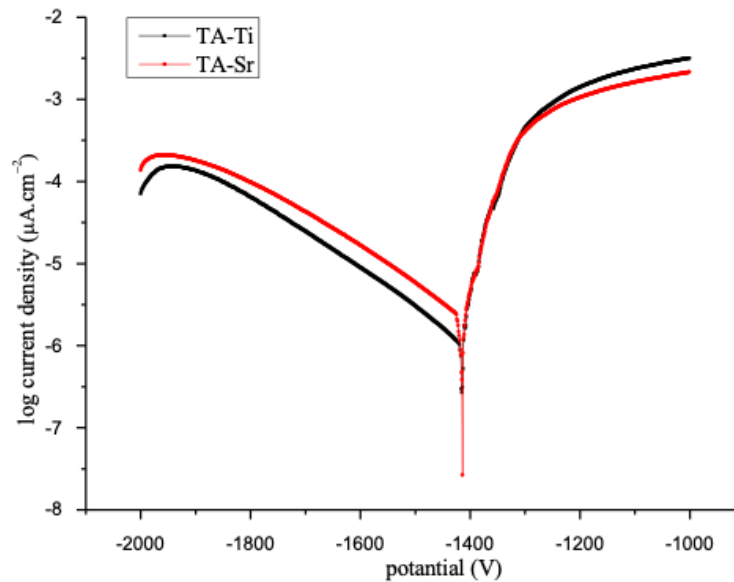
Figure 5. Tafel graphs of TA-Ti and TA-Sr magnesium alloys.

Figure 6 shows the degradation rate graph of TA-Ti and TA-Sr alloys whose degradation rates were calculated by the mass loss method following immersion test. When the graph is examined, it is observed that the degradation rates become stable after about 50 hours. The degradation rate values of the alloys are given in Table 1. As also observed from Table 1, the degradation rate of the TA-Ti alloy (0.18 mm/yr) has a lower value compared to the degradation rate of the TA-Sr alloy (0.24 mm/yr). When the Tafel graph obtained from the electrochemical measurements and the degradation rate graph obtained from the mass loss measurements following the immersion test are examined together, it can be said that both graphs are compatible. The reason for the value of the degradation rate being smaller compared to the value of the corrosion rate is the inability to completely clean the corrosion products remaining within the surface, which transforms into a porous structure during the degradation.
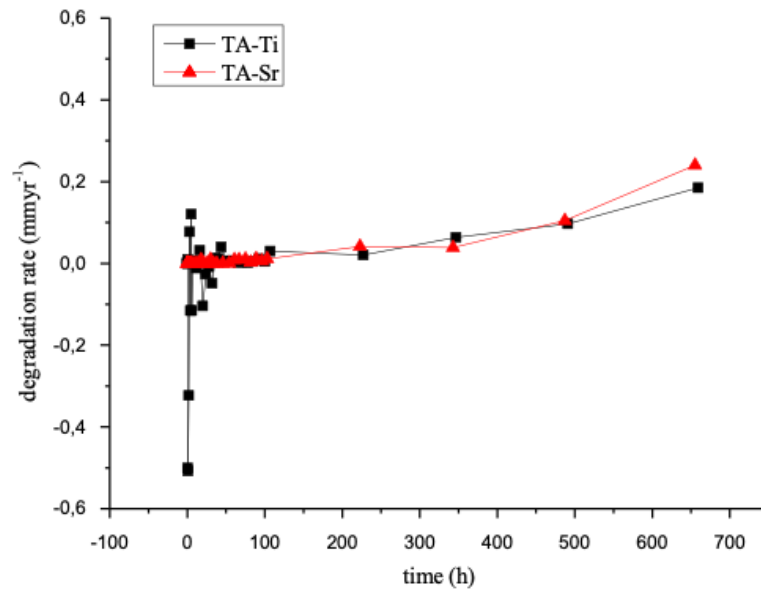
Figure 7. Tafel graphs of TA-Ti and TA-Sr magnesium alloys.

Table 1. Some corrosion parameters of magnesium alloys.

Alloy	E_{corr} (V)	I_{corr} ($\mu A.cm^{-2}$)	Corrosion rate (mm/yr)	Degradation rate (mm/yr)
TA-Ti	-1.415	4.45	3.8	0.18
TA-Sr	-1.414	6.80	5.8	0.24

It is well known that the changes in the microstructure of an alloy affect the alloy's corrosion properties as well as directly affect the alloy's mechanical properties [33-34]. The reduction in grain size by the addition of Ti might have caused the formation of a more passive film and its role in preventing corrosion [35]. As a result of the electrochemical and immersion tests performed, it was observed that the addition of both alloys had the effect of increasing the corrosion resistance of magnesium, but that the addition of Ti was more effective in enhancing the corrosion.

4. DISCUSSION

The microstructural, mechanical, and corrosion properties of TA-Ti and TA-Sr alloys, produced using the high pressure die casting technique, were investigated. As a result of microstructure examinations, it was observed that the addition of Al-15Ti and Al-15Sr master alloys effectively reduced the grain

size of the Mg-5Sn alloy, and that the addition of Ti was more effective in the reduction of grain sizes compared to the addition of Sr. The alloys were found to be composed of α-Mg phase and Mg_2Sn intermetallic phases. When the mechanical properties were examined, it was observed that the addition of Ti increased the yield strength, tensile strength, percentage elongation, macrohardness, nanohardness, and elastic modulus values more compared to the addition of Sr. It can be stated that both the corrosion and degradation rates obtained as a result of electrochemical and immersion tests decreased with the addition of Ti, in other words the TA-Ti alloy was more resistant to corrosion compared to the addition of TA-Sr.

ACKNOWLEDGEMENT

REFERENCES

[1] Witte, F., Hort, N., Vogt, C., Cohen, S., Kainer, K.U., Willumeit, R., Feyerabend, F., (2008), Degradable biomaterials based on magnesium corrosion, Curr. Opin. Solid State Mater. Sci., 12, 63 -72.

[2] Moravej, M. and Mantovani, D., (2011), Biodegradable metals for cardiovascular stent application: interests and new opportunities," International journal of molecular sciences, 12 (7), 4250-4270.

[3] Kirkland, N.T., Birbilis, N. and Staiger, M.P., (2012), Assessing the corrosion of biodegradable magnesium implants: a critical review of current methodologies and their limitations. Acta biomaterialia, 8 (3), 925-936.

[4] Staiger, M.P., Pietak, A.M., Huadmai, J. and Dias, G., (2006), Magnesium and its alloys as orthopedic biomaterials: a review, Biomaterials, 27 (9), 1728-1734.

[5] Uddin, M.S., Hall, C., Murphy, P. (2015), Surface treatments for controlling corrosion rate of biodegradable Mg and Mg-based alloy implants," Science and technology of advanced materials, 16 (5), 053501.

[6] Johnson, A.R., Munoz, A., Gottlieb J.L. and Jarrard, D.F., (2007), High dose zinc increases hospital admissions due to genitourinary complications, The Journal of urology, 177 (2), 639-643.

[7] Gu, X., Zheng, Y., Cheng, Y., Zhong, S. and Xi, T., (2009), In vitro corrosion and biocompatibility of binary magnesium alloys, Biomaterials, 30 (4), 484-498.

[8] Song, G., Control of biodegradation of biocompatable magnesium alloys (2007), Corrosion science, 49 (4), 1696-1701.

[9] Liu, X., Sun, J., Yang, Y., Pu, Z., Zheng, Y., (2015), In vitro investigation of ultra-pure Zn and its mini-tube as potential bioabsorbable stent material, Mater. Lett., 161, 53-56.

[10] Liu, H., Chen, Y., Tang, Y., Wei, S. and Niu, G., (2007), The microstructure, tensile properties, and creep behavior of as-cast Mg-(1–10)% Sn alloys, Journal of Alloys and Compounds, 440 (1-2). 122-126.

[11] Marya, M., Hector, L.G., Verma, R., Tong, W., (2006), Microstructural effects of AZ31 magnesium alloy on its tensile deformation and failure behaviors, Mater. Sci. Eng., A, 418, 341-356.

[12] Zheng, Y.F., Gu, X.N., Witte, F., (2014), Biodegradable metals, Mater. Sci. Eng. R. Rep., 77, 1-34.

[13] Homayun, B. Afshar, A., (2014), Microstructure, mechanical properties, corrosion behavior and cytotoxicity of Mg–Zn–Al–Ca alloys as biodegradable materials, J. Alloys Compd., 607, 1-10.

[14] Sunil, B.R., Kumar, T.S.S., Chakkingal, U., Nandakumar, V., Doble, M., et al. (2016), In vitro and in vivo studies of biodegradable fine grained AZ31 magnesium alloy produced by equal channel angular pressing, Mater. Sci. Eng. C, 59, 356-367.

[15] Sun, W., Zhang, G, Tan, L., Yang, K., Ai, H., (2016), The fluoride coated AZ31B magnesium alloy improves corrosion resistance and stimulates bone formation in rabbit model, Mater. Sci. Eng. C, 63, 506-511.

[16] Huang, Z.H., Zhou, N., Xu, J., Li, Y.D. and Li, W.R., (2017), Microstructure and Mechanical Property of Mg-Sn-Al Wrought Magnesium Alloys, In Materials Science Forum Trans Tech Publications Ltd., 898, 97-103.

[17] Bowles, A.L., Blawert, C., Hort, N. and Kainer, K.U., (2004), Microstructural investigations of the Mg-Sn and Mg-Sn-Al alloy systems, Magnesium Technology, ss.307-310.

[18] Koltygin, A., Bazhenov, V. and Mahmadiyorov, U., (2017), Influence of Al–5Ti–1B master alloy addition on the grain size of AZ91 alloy, Journal of magnesium and alloys, 5(3), 313-319,

[19] Luo, A.A., (2013), Magnesium casting technology for structural applications, Journal of Magnesium and Alloys, 1 (1), 2-22.

[20] Banerjee, A., (2013), Process-Structure Relationships of Magnesium Alloys, The University of Western Ontario Graduate Program in Mechanical and Materials Engineering Master thesis.

[21] Ralston, K.D. and Birbilis, N., (2010), Effect of grain size on corrosion: a review, Corrosion, 66 (7), 075005-075005.

[22] Bahmani, A., Arthanari, S. and Shin, K.S., (2020), Formulation of corrosion rate of magnesium alloys using microstructural parameters, Journal of Magnesium and Alloys, 8 (1), 134-149.

[23] Chao, H.Y. Yang, Y. Wang, X. and Wang, E.D., (2011), Effect of grain size distribution and texture on the cold extrusion behavior and mechanical properties of AZ31 Mg alloy, Materials Science and Engineering: A, 528 (9), 3428-3434.

[24] Oliver, W. C. and Pharr, G. M., (2004), Measurement of hardness and elastic modulus by instrumented indentation: Advances in understanding and refinements to methodology, Journal of materials research, 19 (1), 3-20.

[25] Murray, J.L., (1982), The Al− Mg (aluminum− magnesium) system. Journal of Phase Equilibria, 3 (1), 60-74.

[26] Dieter, G.E. and Bacon, D.J., (1986), Mechanical metallurgy (Vol. 3). New York: McGraw-hill.

[27] Wang, Y., Zeng, X., Ding, W., Luo, A. A., Sachdev, A. K., (2007), Grain refinement of AZ31 magnesium alloy by titanium and low-frequency electromagnetic casting. Metallurgical and Materials Transactions A, 38(6), 1358-1366.

[28] Chen, T. J., Wang, R. Q., Ma, Y., Hao, Y., Grain refinement of AZ91D magnesium alloy by Al–Ti–B master alloy and its effect on mechanical properties. Materials & Design, 34, 637-648.

[29] Naik, G. M., Gote, G. D., Narendranath, S., Kumar, S. S., (2012), Effect of grain refinement on the performance of AZ80 Mg alloys during wear and corrosion. Advances in Materials Research, 7(2), 105, 2018.

[30] Kaya, A.A., Çelik, Ç., Türe, Y., Ataman, A., Arkın, E., Palumbo, G., Sorgente, D. and Turan, D., (2017), Elasticity modulus and damping in some novel magnesium alloys, In Proceedings of the 6th International Conference on Magnesium.

[31] Kaya, A.A., Çelik, Ç., Türe, Y., Ataman, A., Arkın, E., Palumbo, G., Sorgente, D. and Turan, D., (2017), New Magnesium Alloys with High Elastic Modulus, International Materials Technologies and Metallurgy Conference Istanbul.

[32] Özarslan, S., Şevik, H. and Sorar, İ., (2019), Microstructure, mechanical and corrosion properties of novel Mg-Sn-Ce alloys produced by high pressure die casting, Materials Science and Engineering: C, 105, 110064.

[33] Cui, Q., Ti, D., Wang, H., Zhang, J., Xu, J., Wang, B., (2019), Effects of grain size and secondary phase on corrosion behavior and electrochemical performance of Mg-3Al-5Pb-1Ga-Y sacrificial anode, J. Rare Earths.

[34] Aung, N.N. Zhou, W., (2010), Effect of grain size and twins on corrosion behaviour of AZ31B magnesium alloy, Corros. Sci., 52, 589.

[35] Öteyaka, M. Ö., Ghali, E., & Tremblay, R. (2012), Corrosion behaviour of AZ and ZA magnesium alloys in alkaline chloride media, International Journal of Corrosion.